Progress in Flight Physics **5** (2013) 3-22
DOI: 10.1051/eucass/201305003
© Owned by the authors, published by EDP Sciences, 2013

COMPARATIVE STUDY OF DIFFERENT TURBULENCE MODELING APPROACHES TO PREDICTION OF TRANSONIC AND SUPERSONIC FLOWS PAST A REENTRY CAPSULE WITH BALANCE FLAPS

A. Garbaruk[1], D. Niculin[1], M. Strelets[1], A. Dyadkin[2], A. Krylov[2], and K. Stekenius[3]

[1]St. Petersburg State Polytechnic University
29 Poytechnicheskaya Str., St. Petersburg 195251, Russia
[2]RSC "Energia"
4A Lenin Str., Korolev 141070, Moscow Region, Russia
[3]TSNIIMASH
4 Pionerskaya Str., Korolev 141070, Moscow Region, Russia

Computations of a turbulent flow past a reentry capsule are carried out with the use of two Reynolds-averaged Navier–Stokes (RANS) models and Delayed Detached-Eddy Simulations (DDES) in a wide range of the free stream Mach number (M_∞ = 0.8–6.0). It is shown that transonic and slightly supersonic mean flows are more sensitive than the high Mach number flows. Other than that, DDES reveals a significant flow unsteadiness and strong oscillations of forces acting on the capsule which may cause an impact on its survivability. A comparison of simulations with the experimental data on mean flow and integral forces demonstrates a fairly good agreement.

1 INTRODUCTION

A reliable Computational Fluid Dynamics (CFD) prediction of turbulent flows past reentry vehicles is a challenging physical and numerical problem. This is caused by several factors which include a complexity of the geometry, a massively separated character of the flow, and its complicated wave pattern. As of today, computational studies of this type of flow are rather limited. Moreover, most of them address the hypersonic flow regimes (see, e. g., [1–4]), whereas moderately

This is an Open Access article distributed under the terms of the Creative Commons Attribution License 2.0, which permits unrestricted use, distribution, and reproduction in any medium, provided the original work is properly cited.

Article available at http://www.eucass-proceedings.eu or http://dx.doi.org/10.1051/eucass/201305003

supersonic and transonic flow regimes, typical for the approach stage of the flight trajectory and known to be most sensitive to a specific choice of turbulence model, are virtually not investigated. Note also that, in this stage, maneuvering capabilities of a reentry vehicle become especially important. This motivates systematic numerical studies aimed at evaluating the performance of the up-to-date turbulence models as applied to exactly these flow regimes. In the present work, an attempt is undertaken to address this issue by computing a flow past a reentry capsule with balance flaps at Mach numbers within the range 0.8–6.0 with the use of three different turbulence modeling approaches (two RANS models and DDES [5]), with a primary objective to assess the model-sensitivity of major dynamic flow characteristics, first of all, forces and moments acting on the capsule.

The rest of the paper is organised as follows. Section 2 presents a general outline of the computations including a description of the capsule geometry, turbulence models used, and computational aspects of the simulations. Then, in section 3, the results obtained are presented and discussed in some detail and a brief description of the experiments is given followed by a comparison of the computations with the experimental data.

2 GENERAL OVERVIEW OF THE COMPUTATIONS PERFORMED

2.1 Reentry Capsule Geometry

Two considered geometries are shown in Fig. 1. The first one (Fig. 1*a*) presents a simplified reentry capsule. It is similar to the capsule used in the Fire II experiments (includes a spherical fore-body and an after-body shaped as truncated cone) and, in addition, has a "bulge" where the capsule engines are located and two balance flaps whose deferential deflection permits an alteration of the angles of attack and the roll-angle along the trajectory, thus widening the capsule's maneuvering capabilities. The capsule diameter, D, is equal to 4.4 m. The second model geometry (Fig. 1*b*) was used in experiments of TSNIIMASH (see subsection 3.2). It has the same shape as the first one but is much smaller ($D_m = 0.075$ m) and is equipped with a cylindrical sting mount ($d = 0.025$ m) for fixing the model in a wind tunnel (WT).

2.2 Physical Modeling

The air flow past the capsule is assumed to be a compressible flow of the perfect gas with a constant specific heats ratio of 1.4, Prandtl number of 0.71, and

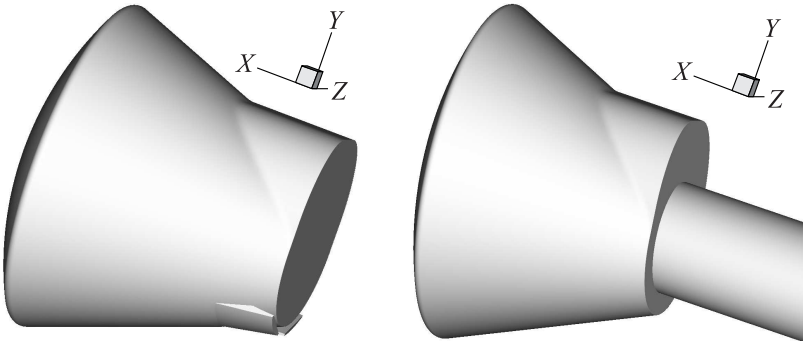

(*a*) (*b*)

Figure 1 Two considered geometries

molecular viscosity depending on temperature in accordance with the Sutherland law. Note that although the perfect gas assumption is not strictly valid at the highest of the considered Mach numbers ($M = 6$), this scarcely may alter conclusions of the study concerning relative capabilities of different turbulence models.

As far as turbulence representation is concerned, major computations are carried out in the framework of the RANS equations coupled with the one-equation Spalart–Allmaras (SA) model with compressibility correction [6] (SACC model) and two-equation k–ω Shear Stress Transport (SST) model of Menter [7], which are currently considered as the most reliable linear RANS models for aerodynamic applications. In addition, some simulations are conducted with the use of a hybrid RANS–LES approach DDES with the SA background RANS model [5]. Delayed detached-eddy simulation presents an enhanced version of the original DES formulation [8]. Particularly, it does not suffer from the so called Modeled Stress Depletion typical of DES performed on "ambiguous" grids, i. e., the grids with tangential cells sizes less than the boundary layer thickness [5]. This advantage of DDES is very important for the considered flow, where the fine tangential grids are used for a correct representation of the geometry and sufficient resolution of the shock waves.

Other than that, in order to get an idea on an impact of a laminar flow "patch" on the spherical fore-body of the capsule which exists even at flight conditions corresponding to very high Reynolds numbers, some of the SACC RANS computations were carried out with the use of two different treatments of the laminar turbulent transition. The first one is a conventional fully turbulent (FT) approach, which assumes that the whole boundary layer on the capsule surface is turbulent, whereas within the second ("tripless" or TL) approach [9]

it is supposed that the flow upstream of the separation is laminar, and the transition to turbulence occurs only in the separated shear layer. Implementation of both approaches is briefly discussed in the next section.

2.3 Computational Domain, Grids, and Boundary Conditions

A computational domain in all the RANS computations was a half-sphere with the diameter of $40D$. The domain, its zoomed fragment and a structured multi-block overset grid of Chimera type in the symmetry plane of the capsule are shown in Fig. 2.

The outer (red) grid block is of O-type, and Cartesian-like (blue and green) blocks are introduced to avoid singularity of the governing equations at the

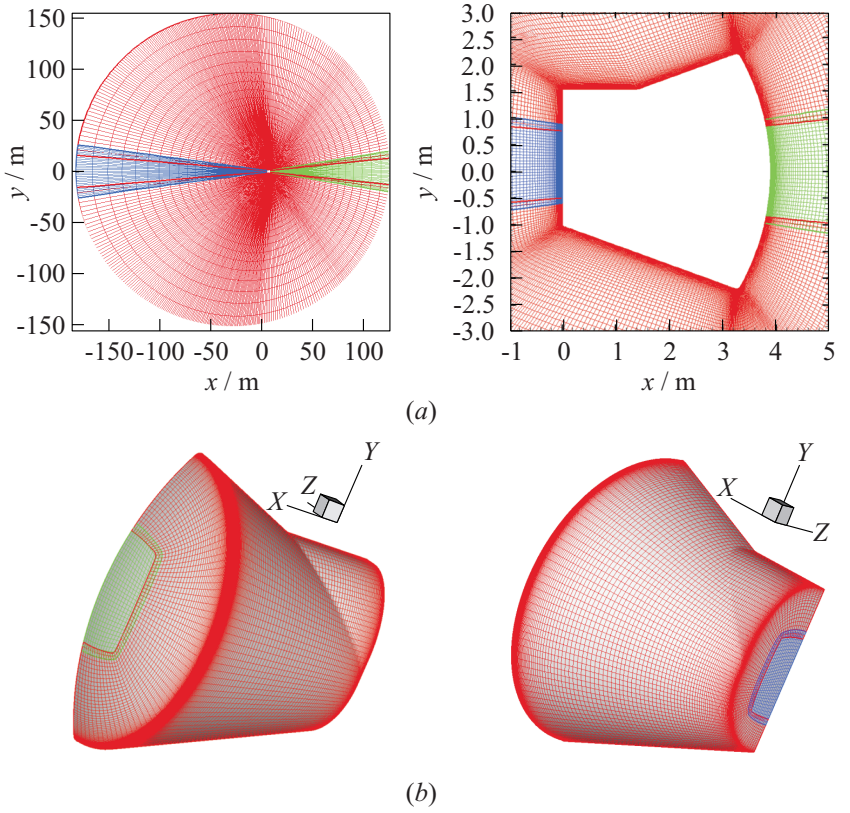

Figure 2 Computational domain and some details of the grid in symmetry plane (a) and on capsule surface (b).

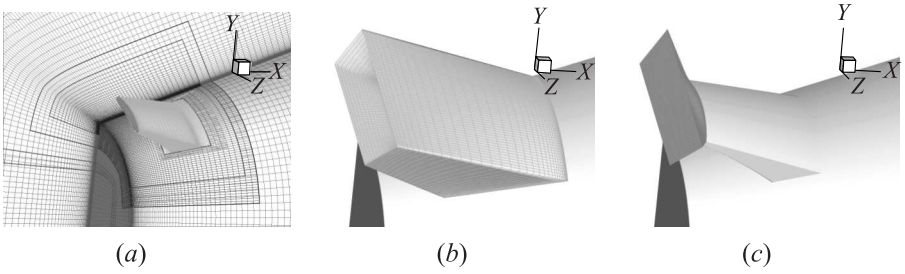

(*a*) (*b*) (*c*)

Figure 3 Some elements of the grid for RANS of the capsule with deflected flaps: (*a*) cutout in the main outer block and flap surface grid; (*b*) flap block; and (*c*) flap blunted edge block

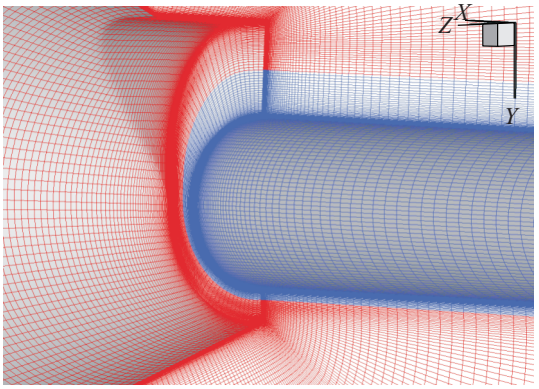

Figure 4 Zoomed grid fragment in the vicinity of the support.

capsule axis. The grid is clustered in the wall-normal direction so that the closest to the wall cell size does not exceed the value of 1 in the wall units ($y_1^+ \leq 1$). Other than that, the grid is refined in the tangential direction in the vicinity of the fore-body/cone and cone/base junctions. A finer resolution in these areas was found to be crucial in the course of preliminary simulations which suggests that otherwise, some peculiarities of the flow patterns (local supersonic zones, shocks and rarefaction waves) cannot be properly represented.

For the cases with deflected balance flaps, additional grid blocks are introduced as illustrated by Fig. 3.

Finally, for the capsule with the cylindrical sting, an additional grid block of O-type is embedded into the main grid block (blue block in Fig. 4).

As far as the DDES grid is concerned, its topology is the same as that of the grid used for RANS, but the computational domain in this case is a whole sphere

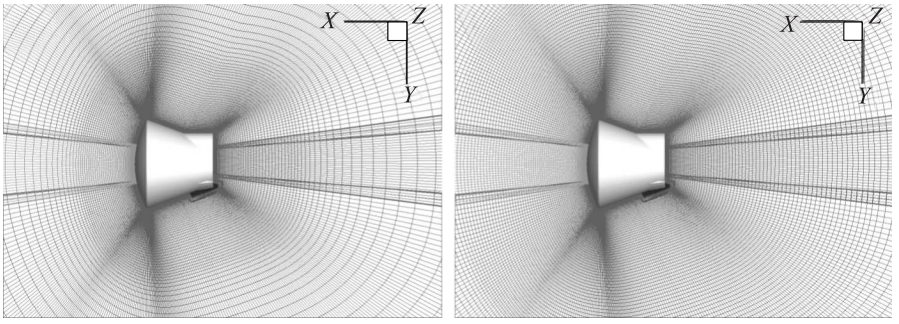

(*a*) (*b*)

Figure 5 Zoomed fragments of computational grids in the symmetry plane used in RANS (*a*) and DDES (*b*)

rather than a half-sphere (for a turbulence-resolving approach the symmetry assumption is not justified). In addition, in accordance with recommendations [10], the grid in the LES region of DDES is significantly refined in the radial direction compared to that used in RANS (Fig. 5). As a result, the DDES grid for the geometry with zero flaps deflection has about 5 million nodes (corresponding half-domain RANS grid has about 2 million nodes), which is close to the practical maximum we could afford with the available computers. For the same reason (restricted computer power) no grid-refinement studies for RANS have been performed. However, computations carried out on considerably coarser grids did not reveal alteration of the obtained solutions comparable with the difference between the predictions of the two considered RANS models. Thus, conclusions regarding the relative models performance formulated based on the computations carried out on the grids shown in Figs. 2–4 may be considered as quite reliable.

Boundary conditions in the computations are imposed as follows.

On the solid walls, nonpermeability and no-slip conditions are used for the velocity vector ($u_w = v_w = w_w = 0$) and the adiabatic condition for the temperature ($\partial T/\partial n|_w = 0$). The modified eddy viscosity on the wall in the SA model transport equation is set equal to zero, whereas within the SST model the turbulent kinetic energy is set zero and its specific dissipation rate is computed as $\omega_w = 10[6\nu/(\beta_1 \Delta y_1^2)$ [7], where ν is the molecular viscosity, $\beta_1 = 0.075$ is the constant of the SST model, and Δy_1 is the first near wall grid step.

At the outer boundary of the computational domain, for the aerodynamic variables, the characteristic boundary conditions are imposed and the turbulent quantities are defined as follows. For the SACC model, the eddy viscosity at the inflow parts of the outer boundary, $\nu_{t\infty}$, is specified. For the SST model, the inflow value of the specific dissipation rate is defined as [7] $\omega_\infty = CU_\infty/D$

(U_∞ is the free stream velocity and the constant $C = 2.5$), whereas the inflow turbulent kinetic energy, k_∞, is computed via ω_∞ and the eddy viscosity $\nu_{t\infty}$: $k_\infty = \rho_\infty \nu_{t\infty} \omega_\infty$. As far as the specific value of the inflow eddy viscosity is concerned, it depends on the approach used for laminar–turbulent transition control. If the FT approach is used, it is set equal to the molecular viscosity; this provides a rapid forming of the developed turbulent boundary layer on the body surface.

In the framework of the TL approach (laminar flow upstream of separation and turbulent flow in the separated shear layer and downstream of separation), computation is performed as follows [9]. First, the same boundary condition is imposed as that within the FT approach ($\nu_{t\infty} = \nu$). This computation is continued until forming a recirculation zone in the leeward region of the capsule. After that, the inflow value of the eddy viscosity is set to a small value ($10^{-3}\nu$), and the computation is continued until a converged steady-state solutions is obtained. As a result, the eddy viscosity in the attached boundary layer is virtually zero (it is "washed out" by convection) and in the recirculation zone and in the wake, the flow remains turbulent.

Finally, at the outflow parts of the outer boundary, all the turbulent quantities are defined by the linear extrapolation from the interior of the domain.

2.4 Numerics

All the computations are carried out with the use of the compressible branch of the in-house NTS code [11]. This is a structured multiblock code well established in the field of modern turbulence-resolving treatments. The code has passed extensive code-to-code comparisons with other public, in-house industrial, and commercial CFD codes (CFL3D of NASA, GGNS of Boeing, ELAN of the Technical University of Berlin, CFX, and FLUENT) and, as of today, is considered as one of the most reliable and efficient research CFD codes for aerodynamic applications.

For compressible steady RANS computations, the code employs an implicit 3rd-order upwind-biased flux difference splitting scheme of the Roe [12] with variable time-step and local flux limiters.

For DDES, a hybrid scheme with a solution-dependent blending function [13] is used. This ensures the functionality of the method as a low dissipation 4th-order central scheme in the LES area of DDES providing sufficient turbulence resolution, and as 3rd-order upwind scheme in its RANS and irrotational areas needed for numerical stability. Time integration is carried out with 2nd-order three-layer backward scheme, and numerical implementation is performed by implicit relaxation algorithms (Plane/Line Gauss–Seidel relaxation for the Navier–Stokes equations and Diagonally Dominant ADI (alternating direction implicit) algorithm for the turbulence transport equations).

2.5 Matrix of Cases

With the use of the methodology briefly outlined above, a wide range of computations have been performed for both flight and WT conditions at different flow regimes (Mach number M = 0.8–6.0, angle of attack, $\alpha = 0°$–$30°$, and flaps deflection angle, $\delta_F = 0°$–$30°$). However, this paper focuses mostly on a few cases which are most revealing in terms of assessment of different approaches to turbulence modeling. These cases are summarized in Table 1.

Table 1 Matrix of cases

Case	Flight/ WT conditions	Altitude, km	Mach number	Reynolds number	α	δ_f	Turbulence treatment	Transition treatment
1	Flight	15	0.8	$1.42 \cdot 10^7$	20°	10°	SACC RANS	FT
2	Flight	15	0.8	$1.42 \cdot 10^7$	20°	10°	SST RANS	FT
3	Flight	15	0.8	$1.42 \cdot 10^7$	20°	10°	SA DDES	FT
4	Flight	15	0.8	$1.42 \cdot 10^7$	20°	0°	SACC RANS	FT
5	Flight	15	0.8	$1.42 \cdot 10^7$	20°	0°	SST RANS	FT
6	Flight	15	0.8	$1.42 \cdot 10^7$	20°	0°	SA DDES	FT
7	Flight	40	6.0	$2.09 \cdot 10^6$	20°	0°	SACC RANS	FT
8	Flight	40	6.0	$2.09 \cdot 10^6$	20°	0°	SST RANS	FT
9	WT	—	0.8	$1.54 \cdot 10^6$	20°	0°	SACC RANS	FT
10	WT	—	0.8	$1.54 \cdot 10^6$	20°	0°	SACC RANS	TL

3 RESULTS AND DISCUSSION

3.1 Turbulence Model and Transition Control Sensitivity

Simulations performed have shown that the effect of turbulence model on predicted mean flow characteristics and integral forces acting on the capsule is most pronounced for the transonic and slightly supersonic flow regimes. As an illustration, in Figs. 6 and 7 comparison of results obtained with the use of three different approaches to turbulence representation at M = 0.8 (cases 1–3 in Table 1) is shown.

The figure reveals a noticeable difference between the RANS solutions with the SACC and SST turbulence models (e. g., the recirculation zone predicted by the SST model is tangibly shorter than that predicted by the SACC model). However, as could be expected for a massively separated flow, the difference between the both RANS solutions and DDES predictions is much larger that between the two RANS models. In particular, the pressure, Mach number and

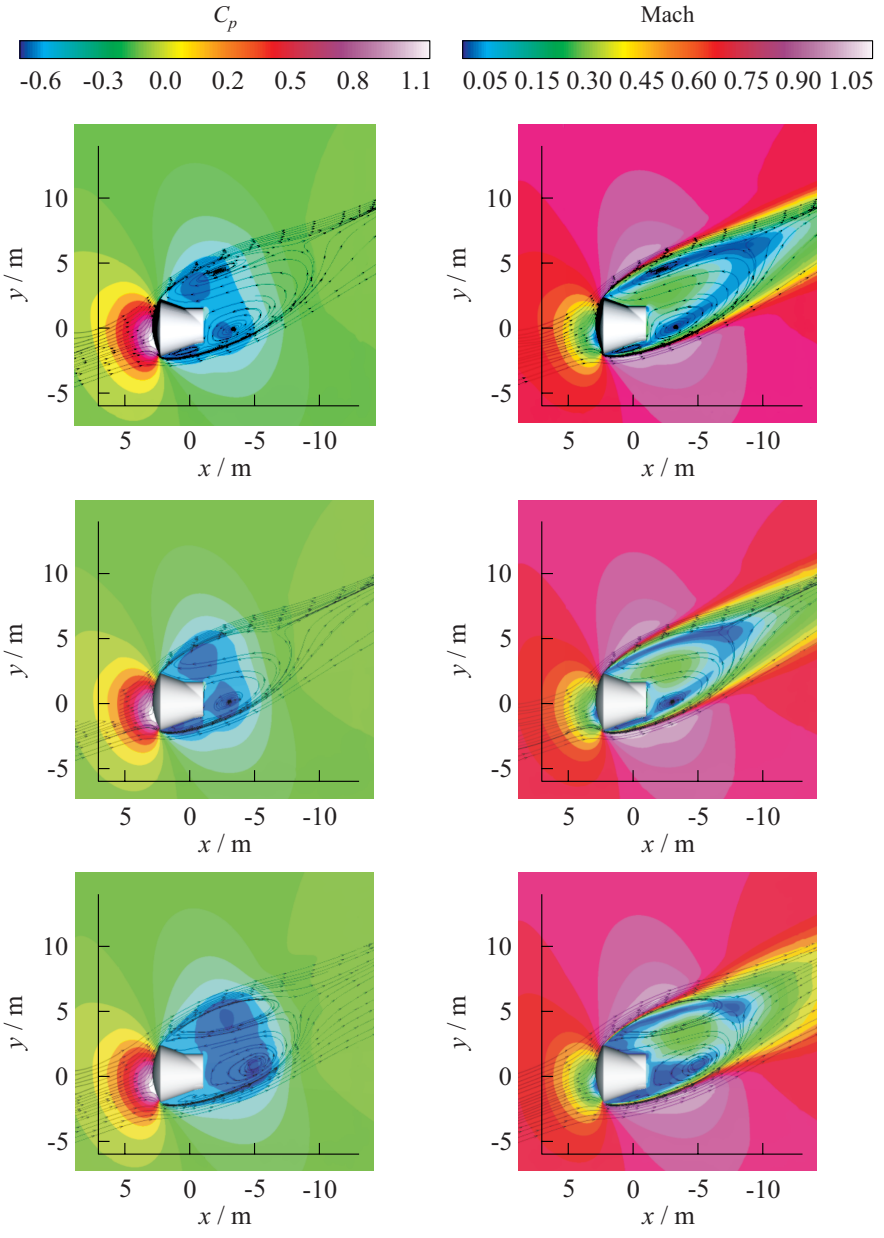

Figure 6 Comparison of streamlines and contours of mean pressure (a) and Mach number (b) in symmetry plane from SACC RANS (upper row); SST RANS (middle row); and SA DDES (lower row). Cases 1–3 from Table 1.

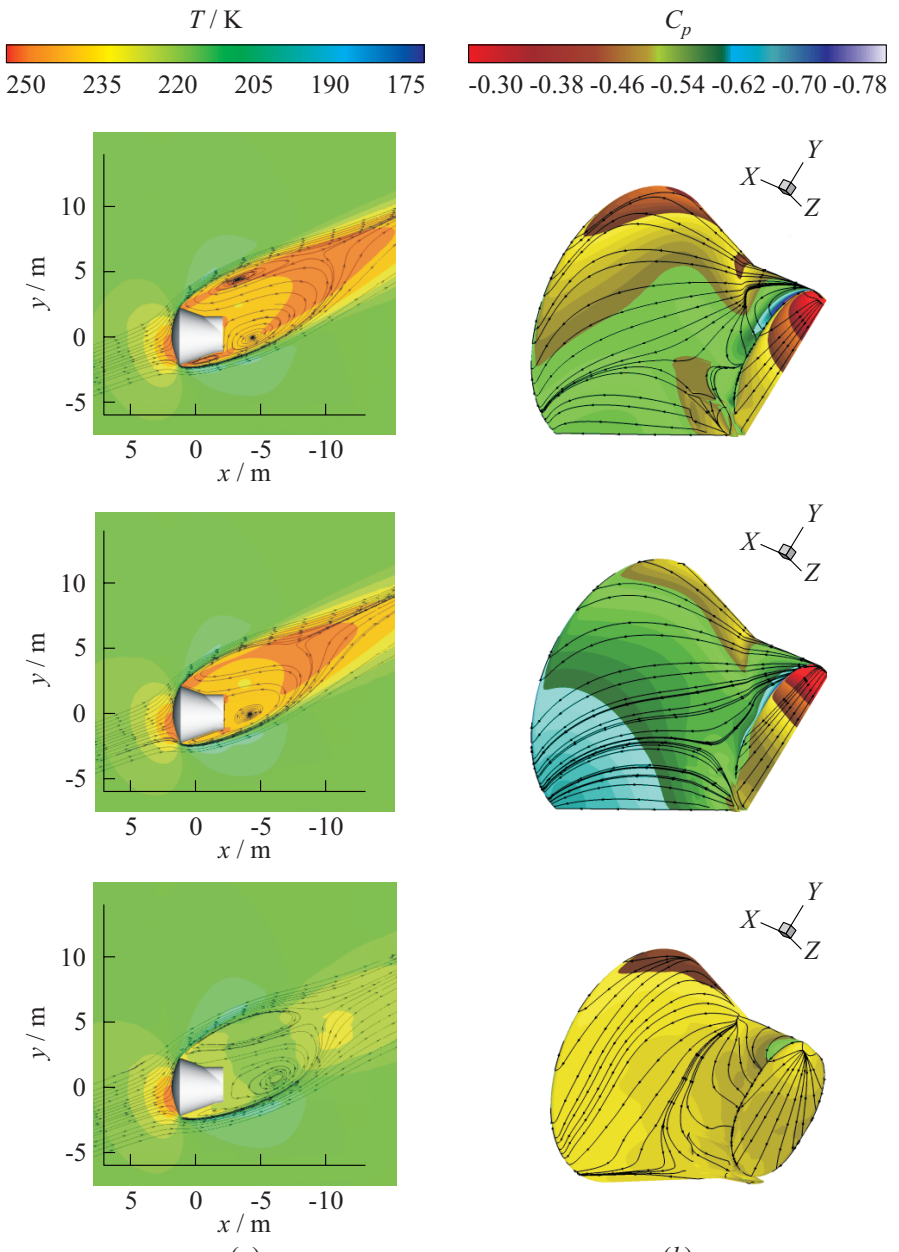

Figure 7 Comparison of temperature (a) in symmetry plane and surface pressure and streamlines ("oil flow") (b) from SACC RANS (upper row), SST RANS (middle row), and SA DDES (lower row). Cases 1–3 from Table 1.

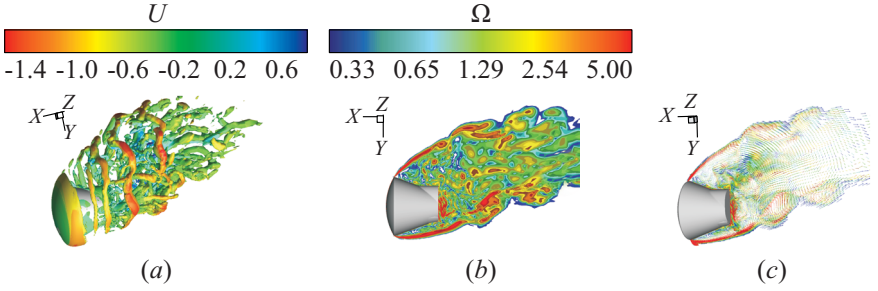

Figure 8 Instantaneous swirl isosurface coloured by streamwise velocity (a), contours of vorticity magnitude in the symmetry plane (b), and velocity vectors in the symmetry plane coloured by vorticity magnitude (c) from DDES of $M = 0.8$ flow (Case 3 in Table 1).

temperature fields in the symmetry plane of the wake and, especially the surface pressure predicted by DDES, are much more uniform than those predicted by RANS. This observation is consistent with results of RANS and DES computations of the supersonic base flow [14, 15].

The reason of observed differences between the RANS and DDES predictions is a complicated three-dimensional (3D) unsteady vortical structure of the wake flow shown in Fig. 8. One can see that it is characterized by the presence of relatively large vortical rings and streamwise vortices (Fig. 8a) and by fine-grained turbulent eddies (Figs. 8b and 8c), i. e., by the features that cannot be captured by a RANS model of any level of complexity.

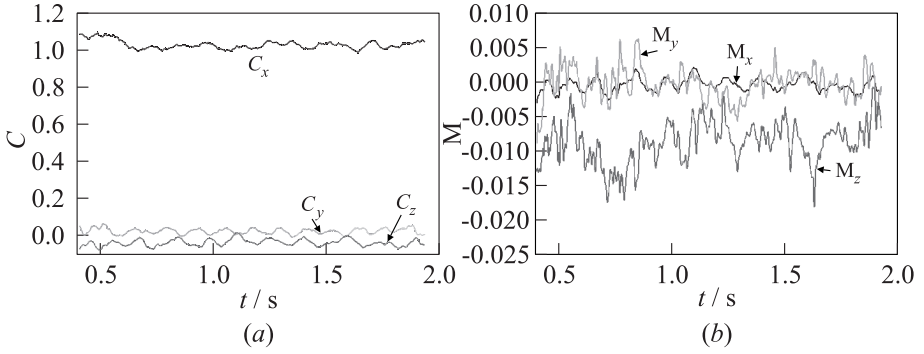

Figure 9 Time variation of coefficients of integral forces (a) and moments (b) from DDES (Case 3 in Table 1)

Table 2 Effect of turbulence model on integral forces and moments acting on the capsules with deflected flaps

Case	Turbulence treatment	C_x	C_y	C_z	C_y/C_x	M_x	M_y	M_z
1	SACC RANS	1.0082	−0.351	0	−0.349	0	0	−0.015
2	SST RANS	1.0394	−0.383	0	−0.369	0	0	−0.014
3	SA DDES	1.0117	−0.309	−0.006	−0.306	−0.0005	−0.004	−0.002

Table 3 Effect of turbulence model on integral forces and moments acting on the capsule with zero flaps deflection

Case	Turbulence treatment	C_x	C_y	C_z	C_y/C_x	M_x	M_y	M_z
4	SACC RANS	1.0077	−0.351	0	−0.348	0	0	−0.016
5	SST RANS	0.9941	−0.361	0	−0.363	0	0	−0.013
6	SA DDES	0.9999	−0.310	−0.006	−0.310	−0.0005	−0.004	0.000

As a result, instantaneous integral forces and, especially, moments predicted by the DDES experience strong oscillations (Fig. 9). Note that although the range of the frequencies of these oscillations resolved by DDES will be widening with grid-refinement (higher frequencies will be resolved), this should not affect the frequencies addressed on the current grid since the turbulence spectra in the LES region of DDES (not shown) have a visible inertial (obeying the $-5/3$ law) region.

The values of mean integral forces and moments acting on the capsule as predicted by the different turbulence models are given in Table 2. One can see that they differ quite noticeably but not drastically, which might be caused by the dominance of the large shock induced pressures. Quite similar results were o btained for the cases 4, 5, and 6 from Table 1 corresponding to the capsule with zero flaps deflection (Table 3).

In contrast to the transonic flow regime $\mathrm{M} = 0.8$ discussed above, at $\mathrm{M} = 6$ SACC and SST RANS, predictions of the flow- and wave-patterns over the capsule turn out to be very close to each other (Figs. 10–12). This suggests that at the high supersonic and hypersonic flight conditions the effect of RANS turbulence model is insignificant. Unfortunately, due to the computer time restrictions, DDES of the M=6 flow has not been carried out. This does not allow drawing a definite conclusion on the difference between DDES and RANS, but it can be expected that it is also less pronounced than in the case of transonic flow regimes.

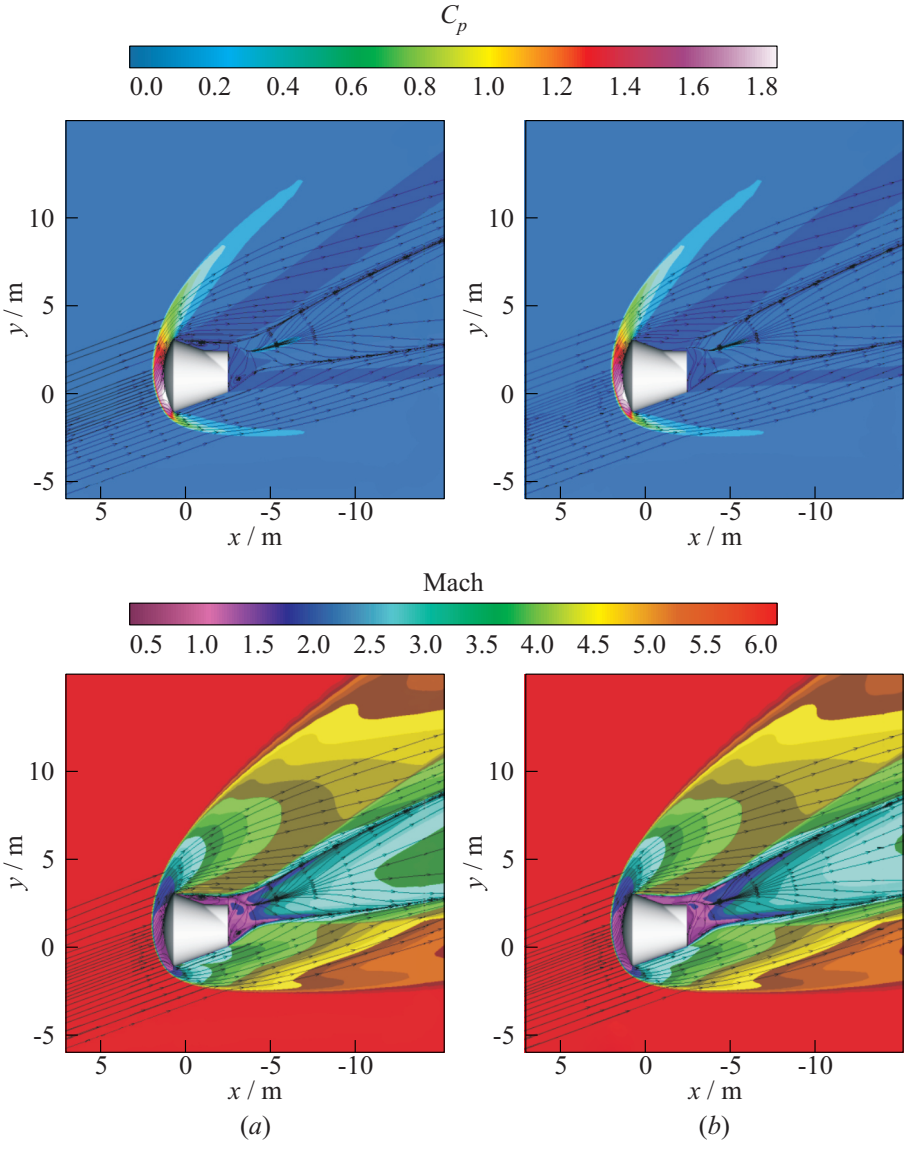

Figure 10 Comparison of streamlines, contours of mean pressure, and Mach number in the symmetry plane from SACC RANS (*a*) and SST RANS (*b*). Cases 7 and 8 in Table 1.

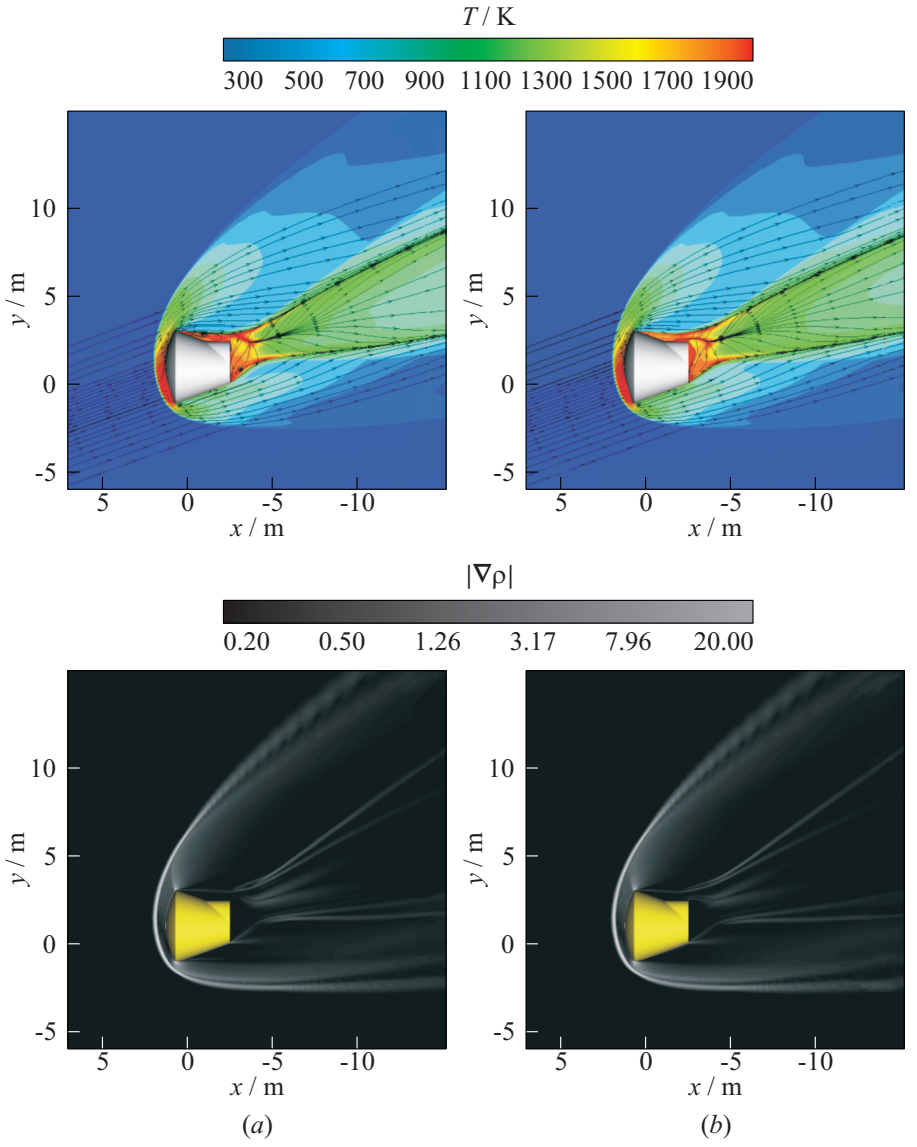

Figure 11 Comparison of temperature and magnitude of density gradient (numerical Schlieren) in the symmetry plane from SACC RANS (*a*) and SST RANS (*b*). Cases 7 and 8 in Table 1.

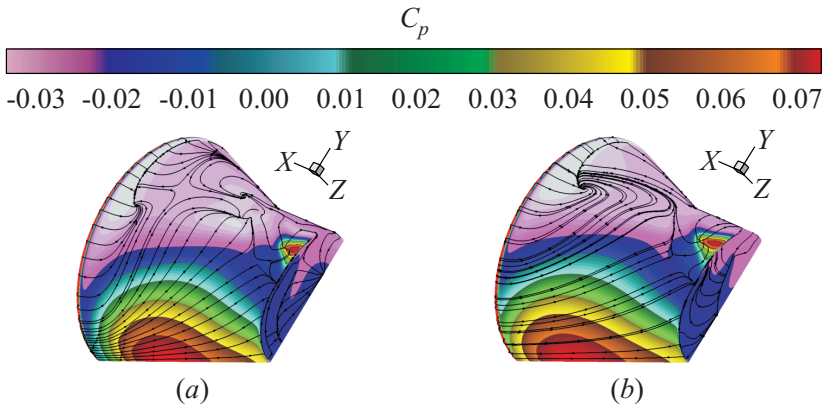

Figure 12 Comparison of surface streamlines ("oil flow") and pressure contours from SACC RANS (a) and SST RANS (b). Cases 7 and 8 in Table 1.

In addition to the turbulence modeling itself, an important aspect of numerical simulations of the considered flow is a treatment of the laminar-turbulent transition, the more so that due to a significant difference of the Reynolds numbers at flight and WT conditions, the transition process in flight and in experiments may be considerably different. As already mentioned, in order to assess a sensitivity of the predictions to the transition treatment, in the present study two approaches to its control in the simulations have been used, the first (FT) assuming a fully turbulent flow past the whole capsule and the second (TL) supposing that the flow upstream of separation is laminar and transition to turbulence occurs in the separated shear layer.

A comparison of results obtained with the use of these two approaches at the WT conditions (Cases 9 and 10 from Table 1), i. e., when the flow in the fore-body boundary layer is most likely laminar, is presented in Fig. 13. It shows that in line with designs of the TL and FT approaches, in the first case the eddy viscosity shows up only downstream of the separation, whereas in the second case it is nonzero all over the fore-body boundary layer. However, even with the FT approach, due to the strong flow acceleration, the boundary layer remains close to laminar (the eddy viscosity is less than the molecular one). Other than that, the minor difference between the eddy viscosity fields in the fore-body boundary layer does not cause any noticeable alteration of the surface pressure and surface streamlines topology (see Fig. 11c, d). Thus, at least for the considered geometry and flow regimes, a more simple FT approach to the transition control seems to be fully justified.

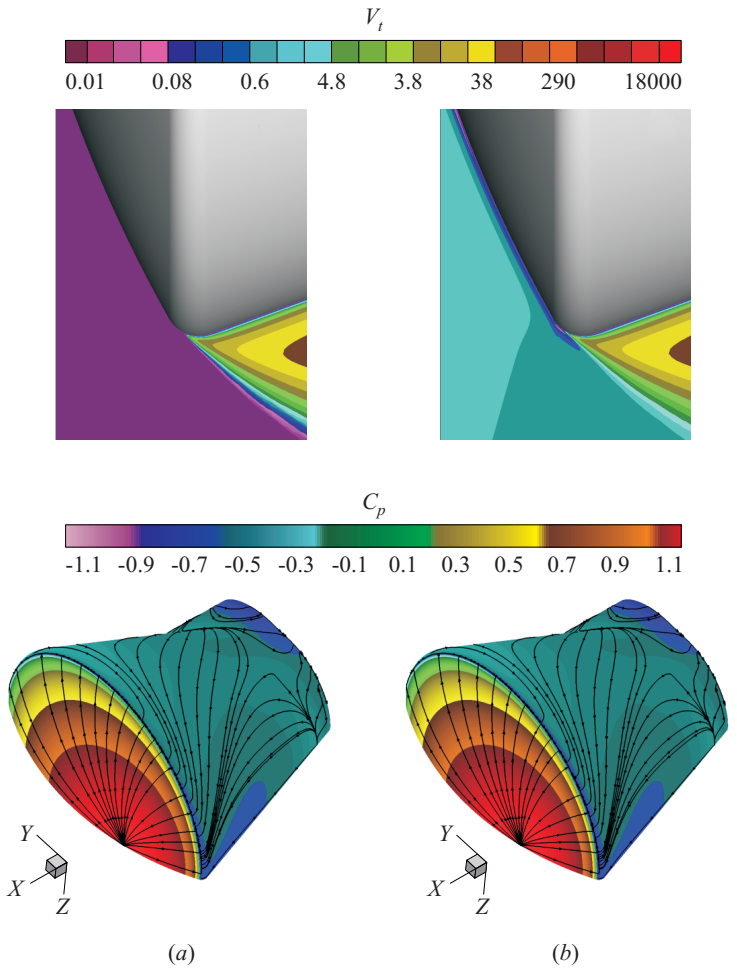

Figure 13 Comparison of TL (a) and FT (b) SACC RANS prediction at M = 0.8 (Cases 9 and 10 in Table 1). Upper row refers to zoomed fragments of eddy viscosity near the fore-body/cone junction, and lower row refers to surfaces streamlines and pressure contours.

3.2 Comparison with Experiment

The experimental study has been carried out in the wind-tunnels U-3M, U-4M and U-303-3 of TSNIIMASH for the model geometry (see Fig. 1) manufactured by the RKK "Energia." The Mach number, Reynolds number based on the model diameter, and angle of attack in the experiments varied within

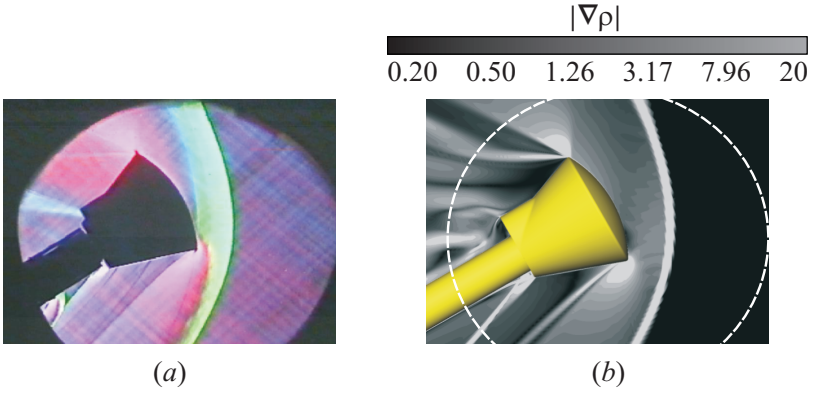

Figure 14 Experimental (a) and numerical (b) Schlieren pictures of the flow M = 1.5, Re = $1.9 \cdot 10^6$, and angle of attack 30°. Dashed white line shows experimental window.

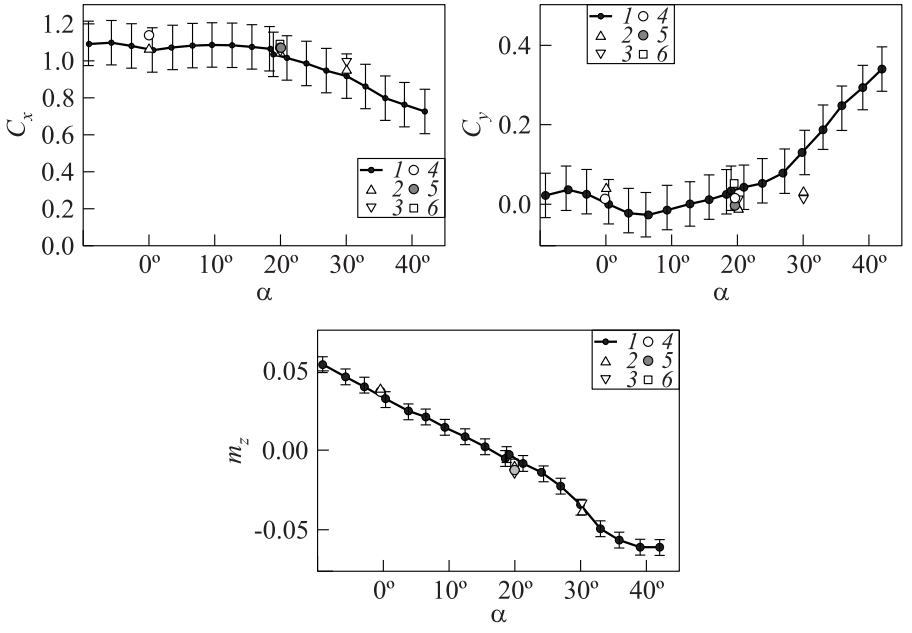

Figure 15 Comparison of predicted and measured coefficients of integral forces and moments at M = 0.8: *1* — experiments, WT, with sting, Re = $1.54 \cdot 10^6$; *2* — SACC RANS, WT, with sting, Re = $1.54 \cdot 10^6$; *3* — SACC RANS, WT, without sting, Re = $1.54 \cdot 10^6$; *4* — SACC RANS, flight, Re = $14.2 \cdot 10^6$; *5* — SST RANS, flight, Re = $14.2 \cdot 10^6$; and *6* — SA DDES, flight, Re = $14.2 \cdot 10^6$

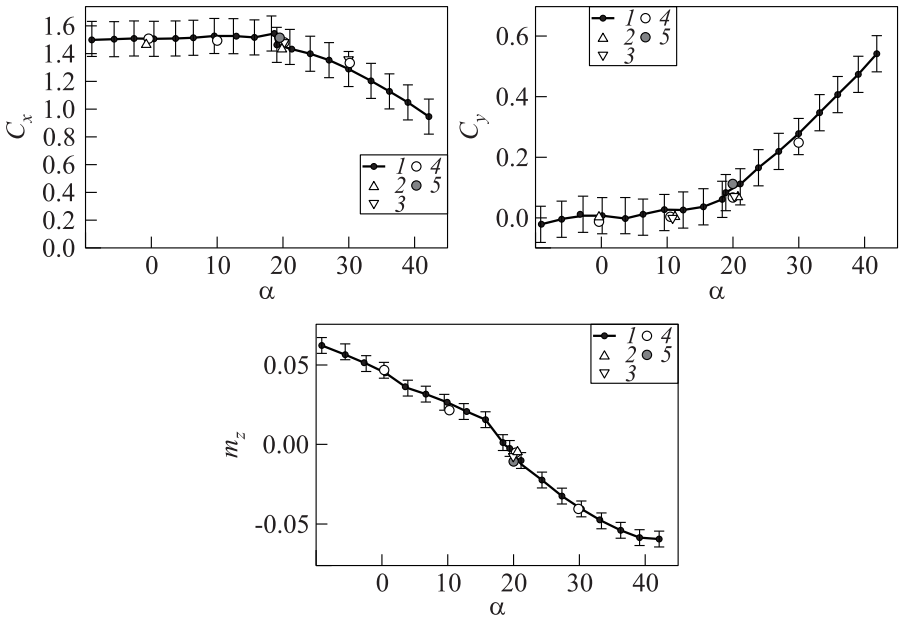

Figure 16 Comparison of predicted and measured coefficients of integral forces and moments at M = 1.5: *1* — experiments, WT, with sting, $\mathrm{Re} = 1.91 \cdot 10^6$; *2* — SACC RANS, WT, with sting, $\mathrm{Re} = 1.91 \cdot 10^6$; *3* — SACC RANS, WT, without sting, $\mathrm{Re} = 1.91 \cdot 10^6$; *4* — SACC RANS, flight, $\mathrm{Re} = 4.1 \cdot 10^6$; and *5* — SST RANS, flight, $\mathrm{Re} = 4.1 \cdot 10^6$

the ranges 0.27–7.7, $(7.1–27) \cdot 10^5$, and 0°–40°, respectively. The integral forces and moments acting on the capsule were measured with the use of an internal six-component strain unit with the errors not exceeding ±0.02 for the drag coefficient, ±0.01 for the lift coefficient, and ±0.001 for the z-component of the moment coefficient. In addition, in the course of experiments Schlieren pictures of the flow were made.

Figure 14 compares experimental Schlieren picture with the numerical one (contours of the magnitude of the density gradient) computed with the use of the SACC turbulence model. The figure suggests that the computation does capture all the details of the flow wavepattern observed in the experiment. Similar results (not shown) are obtained with the use of the SST RANS and DDES.

Finally, Figs. 15–17 present a comparison of the measured coefficients of integral forces and moments with those predicted by the different turbulence models for all the considered flow regimes at flight and experimental conditions (for the latter, the computations were performed both with and without sting). As seen in the figure, all the predictions are well within the range of the experimental uncertainty.

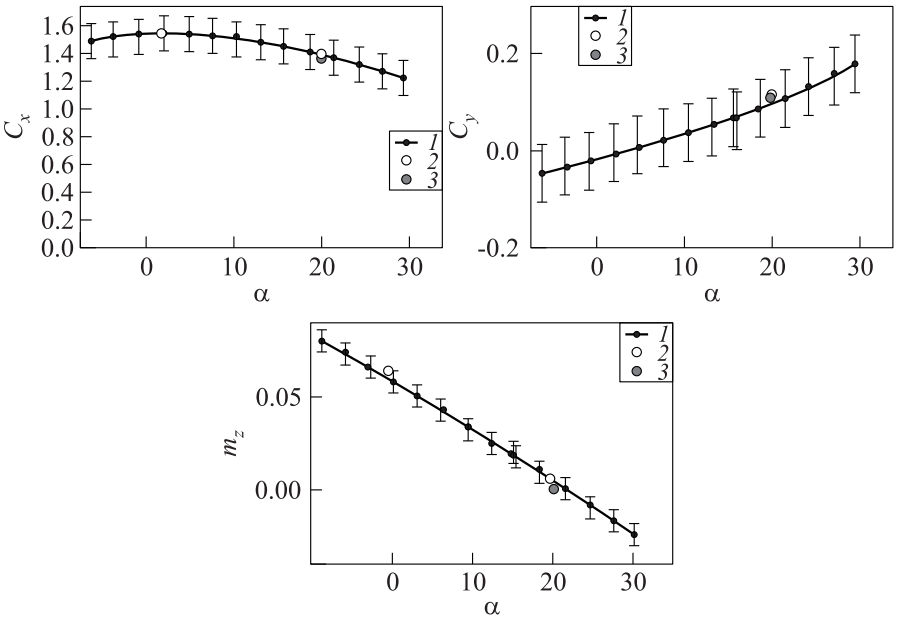

Figure 17 Comparison of predicted and measured coefficients of integral forces and moments at M = 0.6: *1* — experiments, WT, with sting, Re = $2.366 \cdot 10^6$; *2* — SACC RANS, flight, Re = $2.09 \cdot 10^6$; and *3* — SST RANS, flight, Re = $2.09 \cdot 10^6$

4 CONCLUDING REMARKS

Reynolds-averaged Navier–Stokes (with the SACC and SST turbulence models) and SA-based DDES computations are performed of the reentry capsule with and without balance flaps. Results obtained reveal a tangible sensitivity of the mean flow predictions to the turbulence modeling approaches at the transonic and slightly supersonic flow regimes and their marginal sensitivity to turbulence model at the higher Mach numbers (M = 3–6).

However, as of today, it is difficult to give a definite preference to any of the considered approaches because of the considerable scatter of the experimental data on the integral forces acting on the capsule and absence of data for field flow parameters. It can only be stated that all the models are capable of predicting the mean flow characteristics of the flow past the reentry capsule and the integral forces and moments within the experimental scatter. The DDES approach provides, in addition, valuable information on the unsteady loads on the capsule.

REFERENCES

1. Longo, J. M. A. 2004. Modelling of hypersonic flow phenomena. In: *VKI-RTO Lecture Series "Critical technologies for hypersonic vehicle development technology*. Belgium: VKI. RTO-EN-AVT-116.
2. Sinha, K., M. Barnhardt, and G. V. Candler. 2004. Detached eddy simulation of hypersonic base flows with application to Fire II experiments. AIAA Paper No. 2004-2633.
3. Kushal, S., and K. Sinha 2006. Effect of compressibility corrections to turbulence models applied to a hypersonic re-entry configuration. *33rd National and 3rd International Conference on Fluid Mechanics and Fluid Power Proceedings*. Bombay, India. Vol. II. NCFMFP 2006–1221.
4. Sinha, K., and C. Vadivelan. 2008. Effect of angle of attack on re-entry capsule afterbody flowfield. AIAA Paper No. 2008-1282.
5. Spalart, P. R., S. Deck, M. L. Shur, K. D. Squires, M. Kh. Strelets, and A. K. Travin. 2006. A new version of detached-eddy simulation, resistant to ambiguous grid densities. *Theor. Comp. Fluid Dyn.* 20:181–95.
6. Spalart, P. R. 2000. Trends in turbulence treatments. AIAA Paper No. 2000-2306.
7. Menter, F. R. 1993. Zonal two equation k–ω turbulence models for aerodynamic flows. AIAA Paper No. 93-2906.
8. Spalart, P. R., W.-H. Jou, M. Strelets, and S. R. Allmaras. 1997. Comments on the feasibility of LES for wings, and on a hybrid RANS/LES approach. In: *Advances in DNS/LES*. Eds. C. Liu and Z. Liu. Columbus, OH: Greyden Press.
9. Shur, M., P. Spalart., M. Strelets, and A. Travin. 1996. Navier–Stokes simulation of shedding turbulent flow past a circular cylinder and a cylinder with backward splitter plate. *3rd ECCOMAS Computational Fluid Dynamics Conference*. 676–82.
10. Spalart, P. R. 2001. Young person guide to detached eddy simulation grids. NASA/CR-2001-211032.
11. Shur, M., M. Strelets, and A. Travin. 2004. High-order implicit multi-block Navier–Stokes code: Ten-year experience of application to RANS/DES/LES/DNS of turbulence. *7th Symposium on Overset Composite Grid and Solution Technology Proceedings*. Huntington Beach, CA.
12. Roe, P. L. 1981. Approximate Riemann solvers, parametric vectors and difference schemes. *J. Comput. Phys.* 43:357–72.
13. Strelets, M. 2001. Detached-eddy simulation of massively separated flows. AIAA Paper No. 2001-0879.
14. Lüdeke, H., and V. Togiti. 2006. Detached eddy simulation of supersonic shear layer wake flows. *Conference (International) on Boundary and Interior Layers*. Göttingen, Germany.
15. Garbaruk, A., M. Shur, M. Strelets, and A. Travin. 2008. Supersonic base flow. *A European Effort on Hybrid RANS-LES Modelling. Notes on Numerical Fluid Mechanics and Multidisciplinary Design*. 103:197–206.